Theoretical investigation of the ion-induced polarization-charge influence on resonant charge transfer

I. K. Gainullin ●*

Faculty of Physics, Moscow State University, Leninskie gory 1 # 2, Moscow 119992, Russia

This work addresses the modeling of the resonant neutralization of positive alkali-metal ions near metal surfaces. Usually the charge, induced by a positive ion, is taken into account by means of point image charge, located symmetrically to the image plane. Such an approach describes the ion level shift near the metal surfaces and gives reasonable values of the alkali-metal ion neutralization probability on the surfaces with a projected band gap, e.g., Au(111), Cu(111), and Ag(111). In this paper, we show that the induced charge is better described by means of a negatively charged plane located near the surface. This charged plane forms a potential barrier, the inclusion of which in the numerical model significantly reduces the calculated electron transfer probability and allows us to reach quantitative agreement with experimental data for free-electron surfaces, e.g., Cu(110). This repulsive potential barrier generates ion-induced states, by means of which the resonant neutralization of positive alkali-metal ions on free-electron surfaces occurs. Ion-induced states are not so important for surfaces with a projected band gap, because in this case ion neutralization occurs via well-known surface states.

I. INTRODUCTION

Ion beams are widely used for the diagnosis of solids, controlled surface modification, the development of functional coatings, cancer treatment, and other problems associated with analysis and modification of the properties of physical objects at the atomic level [1–17]. The physical processes that occur during an ion-surface interaction are usually classified according to the form of energy transfer into elastic and inelastic. Elastic processes include ion scattering, sputtering of surface atoms, and surface modification. Inelastic processes are characterized by interaction with the electronic subsystem, including electron exchange, electron emission, and ion stopping due to the excitation of the electronic subsystem.

The investigation of resonant charge transfer (RCT) during ion beam scattering and surface sputtering, i.e., energy-conserving one-electron tunneling through the potential barrier between an atomic particle and the surface, is of fundamental and practical importance in several branches of physics and chemistry [18,19], including surface analysis, surface reactivity and catalysis, development of negative ion sources, etc. For example, low-energy ion scattering (LEIS) is known as a technique with the best surface sensitivity [20–22]. Ignoring or incorrectly accounting for the ion neutralization leads to a significant error in the surface composition analysis [23]. The alkali-metal ions are widely used in LEIS; their neutralization near metal surfaces occurs resonantly [24]. RCT has been extensively investigated both experimentally and theoretically over the past few decades [25–48]. There are many excellent reviews on this subject [24,49–52].

The RCT is very sensitive to the electronic structure of the surface. In the case of surfaces with a so-called *projected band gap*, surface and image potential states play a dominant role in electron transfer [32,53,54]. The electronic surface states are formed due to the sharp transition from solid material to vacuum [55,56]. The usual classification distinguishes between (i) *intrinsic surface states* for clean and well-ordered surfaces, which originate from the material to vacuum transition; and (ii) *extrinsic surface states* for surfaces with defects and adsorbates. The intrinsic surface states are mainly localized at the surface atomic layer. There are two basic physical models for intrinsic surface-state description: (i) *Shockley surface states* [57] for the near-free-electron approximation; and (ii) *Tamm surface states* for the tight-binding approach [58]. The electron near the metal surface experiences a potential arising from polarization induced in the surface region. The interaction energy of the electron with induced polarization charge is known as the image potential. For some metal surfaces there are also so-called *image potential states* generated by the potential well between an attractive image potential barrier and the repulsive surface barrier [59,60]. The repulsive surface barrier arises for surfaces with a projected band gap, i.e., when an electron with a certain energy cannot penetrate into the bulk, due to the absence of the permitted states for an electron moving along the normal to the surface. On the other hand, the electron cannot leave the metal surface because of self-attraction to the induced positive charge. The image potential states are localized in the vacuum region; their energy corresponds to the projected band gap of the metal. Note that the energy of the *true surface states* should also be located within the projected band gap; these states are localized at the surface. Otherwise, surface states are degenerate with bulk states and penetrate deep into the bulk; such states are called *surface resonances*.

To calculate the ion neutralization probability, the so-called adiabatic approximation is often used, in which it is assumed that the electron transfer rate does not depend on the

*Ivan.Gainullin@physics.msu.ru

projectile's energy and occupation [61]. The final charge state of the projectile can be formally obtained by integrating the semiclassical rate equation. Despite its simplicity, many experimental data and important regularities of electron exchange, including RCT during grazing scattering and neutralization of highly charged ions, were explained using the adiabatic approximation and the rate equation [24,26,27]. The general approach to the description of RCT in scattering ions from a metal surface is based on a solution of the Anderson-Newns Hamiltonian [18,49]. However, the practical applicability of the Anderson-Newns model is limited by the need to calculate the matrix elements of the interaction, for which essential assumptions are used, in particular the adiabatic approximation. In recent years, several implementations of the Anderson-Newns model have been presented, including its application to the problem of alkali-metal ion neutralization on metal surfaces [43–45]. Despite their significant practical importance, these calculations cannot explain some experimental regularities of alkali-metal ion neutralization, for example a high neutralization probability on metals with a low work function for low exit energies. In the past few decades, a wave-packet propagation (WPP) method[1] was developed that has been applied to many RCT problems [32,61,62]. Since the WPP method does not use the adiabatic approximation, it can be used to study the nonadiabatic effects of RCT [63]. Also the WPP method was successfully applied to the problem of alkali-metal ion neutralization [23,63,64]. It should be noted that WPP-based calculations explain the high neutralization probability on metals with a low work function for low exit energies and a nonmonotonic energy dependence of the neutralization probability for the surfaces with a high work function. In general, the RCT with simple metal surfaces is rather well understood; existing theoretical/numerical models reproduce many experiments [24,49,50,52,63–65]. However, for some situations, such as, for example, the relatively simple free-electron Cu(110) surface, the existing theory cannot reproduce experimental data on the alkali-metal ion neutralization probability [23,45]; the relative error is about 50%. The same approach quantitatively describes experiments on the alkali-metal ion neutralization on surfaces with a projected band gap, for example, Cu(111), Ag(111), Au(111), or experiments on the negative ion formation on free-electron surfaces [24,63,64].

For the modeling of the neutralization of positive ions, it is important to take into account the polarization charge induced by the ion. Usually, the induced charge was taken into account by means of point image charge, located symmetrically to the image plane [28,63,64,66]. This approach describes the ion level shift near metal surfaces and gives reasonable values of the alkali-metal ion neutralization probability on surfaces with a projected band gap. In this theoretical work, we show that the induced charge is better described by means of a negative charged plane located near the surface. This charged

plane forms a potential barrier, the inclusion of which in the numerical model significantly reduces the calculated electron transfer probability and allows us to reach a quantitative agreement with experimental data for free-electron surfaces, e.g., Cu(110). This repulsive potential barrier generates ion-induced states by means of which the resonant neutralization of alkali-metal ions on free-electron surfaces occurs. To the best of our knowledge, the existence of true surface states or image potential states was not predicted theoretically or observed experimentally for the free-electron surfaces [i.e., surfaces without a projected band gap near the $\bar{\Gamma}$ point, like Cu(110)]. Note that when RCT is considered, the surface band structure in the center of the surface Brillouin zone at the $\bar{\Gamma}$ point is usually implied, whereas the band structure also depends on the position inside the Brillouin zone. For example, the Cu(110) surface is a free-electron surface near the $\bar{\Gamma}$ point, but it contains an energy gap at the $\bar{Y}$ point; two surface states are localized within this gap near the $\bar{Y}$ point [67]. In this article, we will further consider the band structure near the $\bar{\Gamma}$ point, which is relevant for most of the electron transfer processes, including ion neutralization.

For convenience, the atomic system of units is used, where $m_e = e = \hbar = 1$; e.g., 1 a.u. of distance is equal to 0.53 Å. The energies are given in electronvolts, relative to the vacuum level ($E_v = 0$).

II. THEORETICAL METHODS

In Sec. II A we describe the model for the calculation of the positive alkali-metal ion neutralization probability. In Sec. II B the proper description of ion-induced charge is considered.

A. Calculation of alkali-metal ion neutralization probability

The model of the alkali-metal ion neutralization calculation and numerical methods, used in this research, were described in detail in previous papers [23,63,64,68–70,74]. In brief, we consider the "standard" picture of neutralization of alkali-metal ions on the metal surfaces, where the ion energy level is shifted above the Fermi level due to interaction with image charges [24,49]. Within this picture, neutralization occurs at distances where the ion energy level remains below the Fermi level of metal surface, i.e., $z > z_f$, where z_f is the intersection distance between the ion energy level and the Fermi level (see Fig. 1). The alkali-metal atom is considered a hydrogenlike atom, consisting of a single *active electron* and a screened atomic core. We estimate the neutralization probability, i.e., the "amount of electron" captured by a positive ion, as the amount of electron lost by a neutral atom during the motion along the same trajectory. Initially we calculate survival probability P of a neutral atom leaving the surface by solving the time-dependent Schrödinger equation for outgoing trajectory $z > z_f$. Then $(1-P)$ is used as an estimation for the neutralization probability.

To find the survival probability P, we consider a direct study of the evolution of the active electron wave packet in the compound potential created by the surface and the projectile (the so-called wave-packet propagation method [61,62]; see Fig. 2). Thus, we numerically solve the time-dependent

---

[1]Note that by the WPP method we mean not only its particular realization by Ermoshin and Kazansky, but also other approaches, where the evolution of the active electron in the compound potential created by the surface and the projectile is investigated by direct solution of the Schrödinger equation.
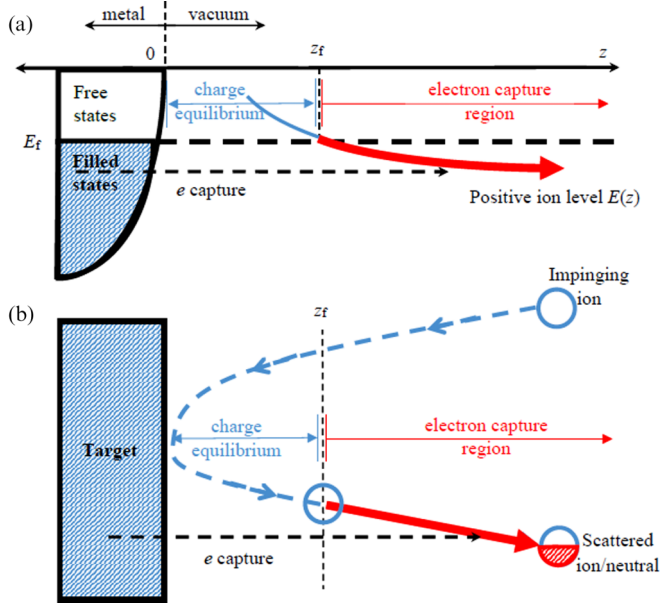
FIG. 1. Illustration of the model of RCT calculation: (a) in energy space; (b) in real space. Details are given in the text.

Schrödinger equation (TDSE) with known initial conditions:

$$i\frac{d\psi(\boldsymbol{r},t)}{dt} = \left(-\frac{\Delta}{2} + U(\boldsymbol{r},t)\right)\psi(\boldsymbol{r},t),$$

$$\psi(\boldsymbol{r},0) = \psi_0(\boldsymbol{r}), \qquad (1)$$

where $U(\boldsymbol{r},t) = V_{e-\mathrm{ion}}(\boldsymbol{r},t) + V_{e-\mathrm{surf}}(\boldsymbol{r}) + \Delta V_{e-\mathrm{surf}}(\boldsymbol{r},t)$ is the time-dependent potential felt by the active electron. Here $V_{e-\mathrm{ion}}(\boldsymbol{r},t)$ describes the electron interaction with the
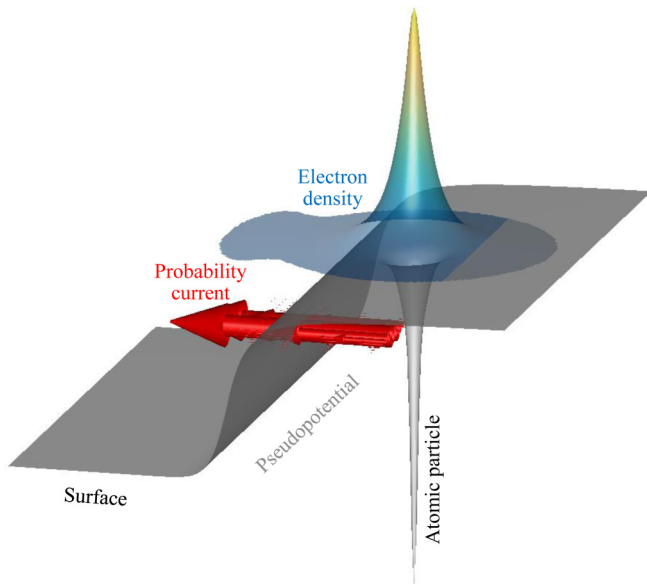

FIG. 2. Illustration of RCT calculation between atomic particle and metal surface. The figure shows (i) the potential, felt by the active electron (gray surface in the lower part); (ii) density of the active electron (color surface in the upper part); (iii) electron flux probability (red arrows). The detailed explanation of the RCT calculation is given in the text.

TABLE I. The parameters of the potential (2) for the sodium cation.

Parameters	Na
p / q	0 / 2
D	1.1
$\alpha_d, /\alpha_q$	0.945/5.0
A_0/ξ_0	10.28159/1.294506
A_1/ξ_1	2.692467/0.681447
A_2/ξ_2	−1.452763/1.0

projectile [71,72], $V_{e-\mathrm{surf}}(\boldsymbol{r})$ describes the electron interaction with the metal surface, and $\Delta V_{e-\mathrm{surf}}(\boldsymbol{r},t)$ describes the interaction with the polarization charge induced by the ion (ion-induced potential; see Sec. II B for details). Note that $U(\boldsymbol{r},t)$ incorporates ion movement, since $V_{e-\mathrm{ion}}(\boldsymbol{r},t)$ implicitly depends on the ion position.

Equation (1) requires potentials for the ion and metal surface. For the ions under study (Li$^+$, Na$^+$, K$^+$), an analytical potential is available [71]. This potential has the following form:

$$V(r) = -\frac{1}{r} - \frac{\alpha_d}{2(r^2+d^2)^2} - \frac{\alpha_q}{2(r^2+d^2)^2}$$
$$+ \sum_l A_l r^p \exp(-\xi_l r^q). \qquad (2)$$

The parameters of the potential (2) for the sodium cation are given in Table I.

Two types of potentials $V_{e-\mathrm{surf}}(\boldsymbol{r})$ are widely used to describe metal surfaces: a "jellium-type" potential for free-electron surfaces [73], and an oscillating potential for the surfaces with a projected band gap [59]. The parameters of these analytical potentials were adjusted to reproduce DFT calculations, as well as the energy of the surface and image potential states. Note that both of these potentials take into account the electron self-attraction to its image charge.

The initial wave packet $\psi_0(\boldsymbol{r})$ is the electronic ground state of an alkali-metal atom, that is, the solution of the time-independent Schrodinger equation (TISE) for a potential $V_{e-\mathrm{ion}}(\boldsymbol{r})$. TISE is also used to find ion-induced states in a given potential (see Ref. [74] for details).

The TDSE numerical solution provides the time evolution of the system's wave-packet $\psi(\boldsymbol{r},t)$. The projection of the current wave function on the initial state $\psi_0(\boldsymbol{r})$ gives the survival amplitude of the wave packet in the initial state:

$$A(t) = \langle \psi_0(\boldsymbol{r}) | \psi(\boldsymbol{r},t) \rangle, \qquad (3)$$

which is a complex function. The square modulus of the survival amplitude gives the survival probability of the initial state, i.e., the probability that the alkali-metal atom is completely neutral:

$$P(t) = |A(t)|^2. \qquad (4)$$

The Laplace transform of the survival amplitude $A(t)$ for a fixed ion-surface distance gives the projected density of states (PDOS) [74].

The final survival probability is formed when the alkalimetal ion/atom moves away from the surface: $P = \lim_{t \to \infty} P(t)$. The initial point of the ion trajectory is $(0, 0, z_f)$, where z_f is the ion-surface distance, where the ion energy level crosses the Fermi level of the metal surface. Note that we consider RCT only for the outgoing trajectory (see the above-described model of alkali-metal ion neutralization calculation). The velocity and direction (angle to the normal) of ion motion are determined according to the experimental conditions. The calculation proceeds until the ion-surface distance reaches 20 a.u., where the electron transfer rate becomes negligible. We consider that the projectile is moving with respect to the surface along a classical trajectory—straight-line motion with constant velocity. Note that the usage of realistic projectile trajectories, which takes into account image-charge attraction, can improve the calculation results to some extent. The trajectory effect is most noticeable for the grazing angle collision (about 10%) and it is decrease significantly for the nongrazing scattering angles [25,31,32].

It should be noted that the above-described model of alkalimetal ion neutralization probability calculation is not *ab initio*, because we calculate the electron loss by a neutral atom instead of the electron capture by a positive ion. Details and the validity of this approach are discussed in Refs. [23,64]. In addition, our model assumes two simplifications: (i) the alkali-metal atom is supposed to be fully ionized at the intersection distance z_f; (ii) we consider only the electron capture strictly for distances $z > z_f$, while the intersection between the ion energy level and the Fermi level is blurred, hence near z_f concurrent processes of electron loss and capture are possible.

As for the first simplification, the positive ion charge near the surface is a natural assumption within the so-called "standard" picture for neutralization of alkali-metal ions on the metal surfaces, where the ion energy level is shifted by the image potential above the Fermi level [49]. But Goldberg and co-workers have shown that for the Li-Cu system, the Li level shifts below the Fermi level at short ion-surface distances [75]. However, recently Gao and co-authors [45] calculated Na^+ neutralization near metal surfaces by means of the modified Brako-Newns model, using the level width provided by Nordlander and Tully [76]. They have shown that at low perpendicular exit energies (up to 2 keV), the alkali-metal ion, neutralized near the surface, becomes completely reionized when it reaches a distance z_f. This fact explains why the assumption of a fully ionized atom at a distance z_f gives correct results for low ion energies.

As for the second simplification, there are three main factors responsible for intersection "blurring." These are (i) the finite ion level width (for example, for an ion-surface distance 10 a.u., the ion level width is about 0.1 eV [76]); (ii) the influence of the ion velocity [24,64]; and (iii) thermal broadening of the Fermi level ($\sim$0.026 eV for room temperature). The consideration of these factors is described in detail in Refs. [23,70]. Of note, the above-described model of the alkali-metal ion neutralization gives reasonable results for ion energies up to 2 keV, which are of practical interest in LEIS experiments.

B. Approach for ion-induced potential

In the previous works on RCT calculation, the ion-induced potential $\Delta V_{e-\text{surf}}(\boldsymbol{r})$ was taken into account as a point negative charge, located symmetrically to the image plane [63,64]. However, this approach does not correctly reflect the RCT dynamics for the problem of the alkali-metal atom ground-state decay in front of the free-electron metal surface. Note that this exact problem is solved numerically to calculate the alkali-metal ion neutralization probability (see Sec. II A). If point negative charge is used for an ion-induced potential $\Delta V_{e-\text{surf}}(\boldsymbol{r})$, the active electron of the alkali-metal atom propagates into the bulk along the normal and is scattered by the ion-induced potential only deep inside the bulk (see the example in Sec. III A). A more realistic approach for the ion-induced potential $\Delta V_{e-\text{surf}}(\boldsymbol{r})$ should take into account the partial reflection of the active electron from the surface plane of the ion-induced negative charge.

In this study, we use a cylindrically symmetric empirical ion-induced potential that incorporates a repulsive potential barrier:

$$\Delta V_{e-\text{surf}}(z, \rho) = \frac{1}{((z+z_{\text{ion}})^2 + \rho^2)^{1/2}} + \frac{\alpha}{|z|}\left(\frac{z_{\text{ion}}}{(z_{\text{ion}}^2 + \rho^2)^{3/2}}\right), \tag{5}$$

where z_{ion} is the distance from the ion to the image plane, and z and ρ are cylindrical coordinates. The ion is located on the axis $\rho = 0$, while $z = 0$ is the image plane.

The first term in Eq. (4) is the classical image potential $1/r'$, where $r' = ((z + z_{\text{ion}})^2 + \rho^2)^{1/2}$ is the distance to the image charge. The second term defines the repulsive potential barrier that is proportional to $1/|z|$ multiplied by the surface density of the induced charge $z_{\text{atom}}/(z_{\text{atom}}^2 + \rho^2)^{3/2}$ [77]. The proportionality coefficient α is the fitting parameter, which has the area's dimension. In all our calculations, we use $\alpha = 10$ a.u.^{2}. This value was obtained by fitting the calculated neutralization probability to the experimental value for 2 keV Na^+ scattering on Cu(110); see Fig. 8 in Sec. III B.

The approximate ion energy level dependence on the ion-surface distance is

$$E_a(z_{\text{ion}}) = V_{e-\text{ion}}(z = z_{\text{ion}}, \rho = 0)$$
$$+ \Delta V_{e-\text{surf}}(z = z_{\text{ion}}, \rho = 0) - 1/4z_{\text{ion}}, \tag{6}$$

where $V_{e-\text{ion}} = E_a(\infty)$ is the ionization energy of the isolated atom, $\Delta V_{e-\text{surf}} = 1/2z_{\text{ion}}$ is the ion level upshift due to the active electron repulsion from the image charge of the ion, and $-1/4z_{\text{ion}}$ is the ion level downshift due to the active electron self-attraction to the image charge. Note that the last term is included in the potential of interaction with metal surface $V_{e-\text{surf}}(\boldsymbol{r})$. After substitution of expression (4) into (5), the ion energy level became

$$E_a(z_{\text{ion}}) = E_a(\infty) + \frac{1}{2z_{\text{ion}}} + \frac{\alpha}{z_{\text{ion}}^3} - \frac{1}{4z_{\text{ion}}}$$
$$= E_a(\infty) + \frac{1}{4z_{\text{ion}}} + \frac{\alpha}{z_{\text{ion}}^3}. \tag{7}$$

Of note, the typical distance of alkali-metal ion neutralization is $z_{\text{ion}} > 8$ a.u. For such distances, the last term of
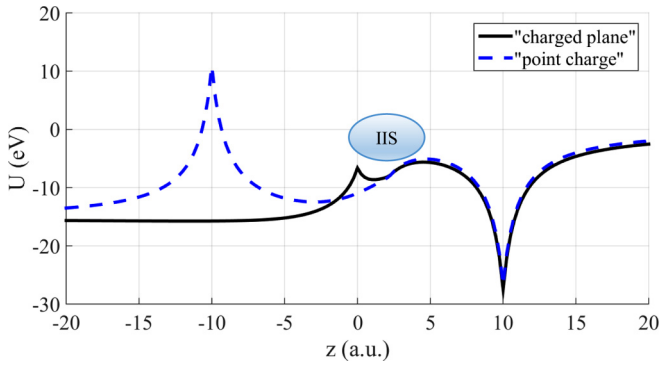
FIG. 3. Sketch of potential relief felt by the active electron for the positive ion, located at 10 a.u. from the image plane of the free-electron metal surface. Black solid line: image/induced charge is taken into account by means of a plane of induced charge; blue dashed line: image/induced charge is taken into account by means of point image charge.

expression (6) is relatively small. Hence, $E_a(z_{ion}) \approx E_a(\infty) + 1/4z_{ion}$, which corresponds to the well-known ion energy level upshift near the metal surface due to the interaction with the image charges [24]. Therefore, the proposed ion-induced potential should not affect previous theoretical results, related to the ion energy level shift due to the interaction with image charges, including the projectile energy gain and the neutralization probability dependence on the surface work function (see Refs. [24,26,27,35], etc.). At the same time, the proposed ion-induced potential affects the RCT rates—it reduces the alkali-metal ion neutralization probability on free-electron surfaces.

It should be noted that when considering the classical distribution of the induced charge in an infinitely thin plane, the Coulomb-like potential barrier $\sim 1/|z|$ does not take place. Nevertheless, a good agreement between the results of calculations using the potential (4) and the experimental data is a strong argument to take into account the repulsive potential barrier, arising due to the ion-induced polarization surface charge. Therefore, we consider the expression (4) as an empirical approach to a realistic ion-induced potential. Possible causes of the appearance of the Coulomb-like potential barrier may be the atomic structure of the surface or the distribution of the induced charge in the near-surface region. If we consider the atomic structure of the metal, then the induced charge will be a set of point charges located on the atoms of the surface layer. In addition, if we take into account the damped oscillations of the induced charge in the surface region [78], the electron has to tunnel through "−/+/−" subsequent regions to exit the surface and neutralize a positive ion. The main objective of this study is to investigate the influence of the repulsive potential barrier on the ion neutralization probability. Since the electron transfer probability depends mainly on the barrier's area, the investigation of the exact barrier shape was not the goal of this article. According to the expression (4), the potential barrier area depends on the fitting parameter α.

Figure 3 illustrates the main features of our approach to the ion-induced potential. The repulsive potential barrier and the electron self-attraction potential form the potential well (black
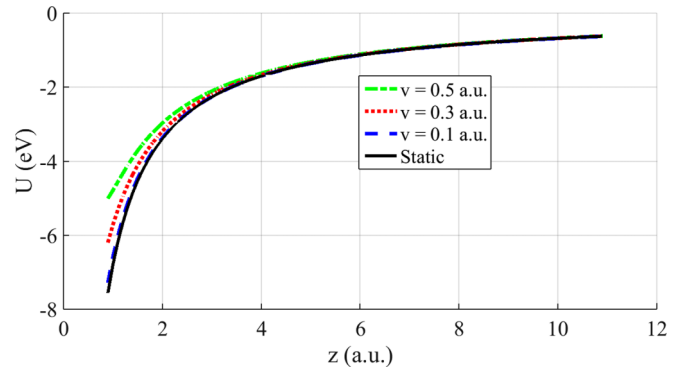

FIG. 4. Image potential of single charge near the Al surface as a function of distance to the image plane for different velocities.

solid line) where ion-induced states (IIS) can arise. Note that IIS are not possible (degenerate with the bulk states) if the induced polarization charge is counted as the point charge (blue dashed line).

It should be noted that we use the classical induced charge surface distribution for a static charge near the surface. For a perfect metal with total screening properties, the image potential of a static single charge is $−1/4z$. The correctness of the classical image potential approach should be verified in the case of moving ions. In Refs. [79,80], a charged particle approaching the solid surface was considered.

For a particle approaching the surface with constant velocity v, the image potential is [80]

$$U(z, v) = \frac{-\omega_s}{2v} f\left(\frac{2\omega_s z}{v}\right), \quad (8)$$

where $f(x) = \int_0^0 \frac{e^{-tx}}{1+t^2} dt$, and ω_s is the surface plasmon frequency.

Figure 4 shows the image potential of a single charge in front of the Al surface ($\omega_s = 0.37$ a.u.) as a function of the distance to the surface for different approaching velocities and classical image potential in the static case. One can see that for the distances of practical interest ($z > 5$ a.u.), the deviations of the "dynamical" image potential from the classical "static" image potential are negligible for ion velocities $v < 0.5$ a.u. Note that a velocity of 0.5 a.u. corresponds to the kinetic energy of alkali-metal ions about dozens of keV, which is significantly higher than the energy of ion beams in LEIS experiments. Therefore, the classical image potential and the surface distribution of induced polarization charge can be used for low-energy ions.

III. RESULTS AND DISCUSSION

RCT simulation results with different models of the ion-induced potential are compared in this section. To make the text more compact, we use the following terms for these models: (i) "point charge"—for the traditional model, when the ion-induced potential is described by the point image charge; (ii) "charged plane"—for our model, when the ion-induced potential is defined according to Sec. II B.
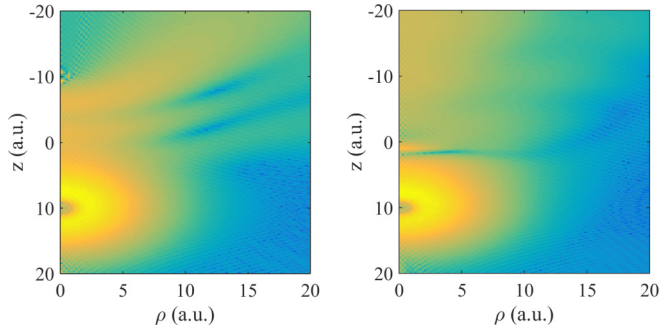
FIG. 5. Electron density of the active electron of Na^0, fixed above Cu(110), at time 100 a.u. after the start of the interaction. The distance to the image plane is 10 a.u. Left-hand side: calculations with "point charge" model. Right-hand side: calculations with "charged plane" model.

A. The influence of ion-induced potential on the RCT process

To compare two approaches for the ion-induced potential, we simulate the static model problem of Na^0 $3s$ electron decay into the Cu(110) surface when Na is fixed in front of the surface. Note that a fair number of similar simulations were presented earlier (see, for example, [32,61,81]), but most of them consider H^- decay, where the ion-induced potential does not arise because of the neutral screened atomic core. Figures 5–7 show the effect of the ion-induced potential on the RCT process. It should be emphasized that Fig. 7 shows survival probability for moving ions, which corresponds to experimental modeling; this is also used in Sec. III B.

The left part of Fig. 5 contains the distribution of electron density, when the point negative charge model is used for an ion-induced potential. Note that for better visualization, we convert 3D electron density distribution $f(x, y, z)$ to 2D distribution $f(z, \rho)$. Initially, the wave packet of the active electron propagates into the metal along the normal to the surface. At $z = -10$ a.u., the wave packet of the active electron is scattered by the point negative image charge. Furthermore, the electron propagates into the bulk along the direction at an angle to the normal.

In the case of a point image charge, the PDOS has a single peak (~ -4.5 eV), corresponding to the Na ground state near the metal surface (dashed blue line in Fig. 6). The evolution of the wave packet in this case is typical for the free-electron surfaces—the electron propagates deep into the metal along the normal, while the Na^0 survival probability $P(t)$ decays exponentially (Fig. 7); a detailed description of "exponential" decay can be found in Ref. [61].

The picture changes dramatically when the "charged plane" model is used for the ion-induced potential (right part of Fig. 5). The plane of the induced negative charge forms a repulsive potential barrier to the electron. Hence, the wave packet of the active electron tunnels through this barrier with certain transmission and reflection coefficients. After passing through the repulsive potential barrier, the wave packet of the electron propagates deep into the bulk, mainly along the normal, while the reflected part of the wave packet continues its movement in the opposite direction. Thus, interference with a forward-moving wave packet occurs. As a result of this
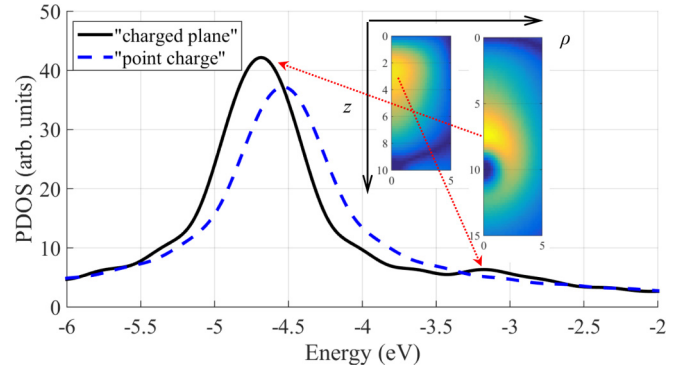

FIG. 6. Projected density of states for the active electron of Na^0, fixed above Cu(110). The distance to the image plane is 10 a.u. Black solid line: calculations with "charged plane" model; blue dashed line: calculations with "point charge" model. The inset shows electron density distributions for "charged plane" model calculations, corresponding to polarized Na ground state (-4.7 eV) and ion-induced state (-3.1 eV).

interference, the electron occupies an ion-induced potential state (see the region with increased electron density in front of the surface on the right-hand side of Fig. 5).

An additional peak of PDOS can be found in Fig. 6 (black solid line), which corresponds to the ion-induced state with an energy of -3.1 eV. This ion-induced state is localized in the vacuum region between the ion and the image plane (see the inset in Fig. 6). The survival probability $P(t)$ in this case exhibits oscillations (see the black solid line at Fig. 7). The above-described picture of RCT with the free-electron Cu(110) surface for the "charged plane" model is very similar to the RCT with surfaces with a projected band gap [32,53,61,65]. Numerous experimental and theoretical studies show that the projected band gap significantly affects RCT and the ion neutralization probability. A typical picture of the H^- decay is that the active electron occupies 2D surface states or image states continua and propagates mainly parallel to the surface. The RCT in this case occurs via surface and image states. In analogy with RCT with the projected
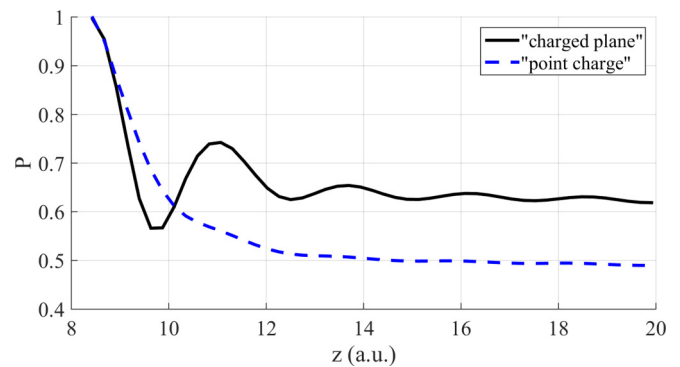

FIG. 7. Survival probability of 2 keV Na^0 leaving Cu(110) surface. The incident angle is 25° to the surface; the exit angle is 28° from the surface. Ion beam energy and geometry correspond to the experiment, described in Ref. [45]. Black solid line: calculations with "charged plane" model; blue dashed line: calculations with "point charge" model.
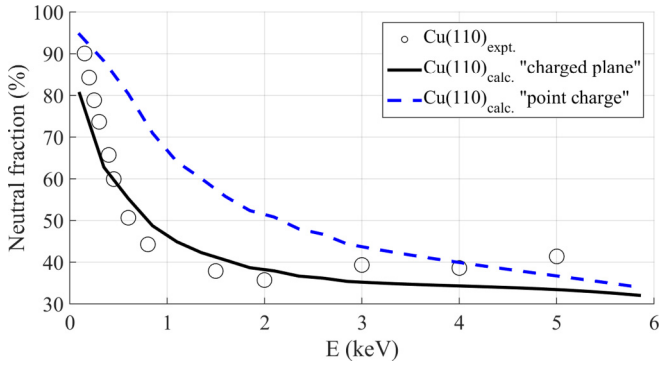
FIG. 8. Comparison of calculations results with experimental data [45]. The figure shows the energy dependence of Na^+ neutralization probability. The primary Na^+ beam is scattered from the Cu(110) surface; the incident angle is 25° to the surface; the exit angle is 28° from the surface. Circles: experimental data; black solid line: calculations with "charged plane" model; blue dashed line: calculations with "point charge" model.

FIG. 9. Comparison of calculations results with experimental data [45]. The figure shows the energy dependence of Na^+ neutralization probability. The primary Na^+ beam is scattered from the Au(111) surface; the incident angle is 67.5° to the surface; the exit angle is 67.5° from the surface. Circles: experimental data; black solid line: calculations with "charged plane" model; blue dashed line: calculations with point image charge.

band-gap surfaces, RCT with positive ions occurs via ion-induced states. Note that ion-induced states should not take place in the case of a neutral or negative projectile core, e.g., H^- formation near metal surfaces [54,65,82].

B. Comparison to experimental data

The way the ion-induced potential is implemented strongly influences the probability of electron transfer in the case of free-electron surfaces. For example, the above-described theoretical model with point image charge describes reasonably well experiments on the alkali-metal ion neutralization on metal surfaces with a projected band gap (see the blue dashed line in Fig. 9 and Ref. [23]), while the discrepancy with the experiment is large for the case of free-electron metals (see the blue dashed line in Fig. 8 and Ref. [23]). However, the proper description of the ion-induced potential significantly improves the agreement between calculation and experiment (see the black solid line in the upper panel of Fig. 8). The reason is that the reflection of the wave packet from the repulsive potential barrier significantly reduces the "amount of electron transferred." As a result, the neutral fraction of Na becomes lower and approaches the experimental data.

It should be noted that the method of ion-induced potential implementation is not so important in the case of surfaces with a projected band gap. The reason is that in this case, the surface potential already includes a potential barrier that reflects the wave packet of the electron. Using the proper ion-induced potential slightly improves the calculation results (see the black solid line in Fig. 9), but this change is not significant. Note that the Na neutral fraction, calculated with the "charged plane" model, has oscillations that are similar to oscillations in experimental data. Such oscillations are probably the result of the reflection of the electron from a complex potential barrier (a combination of the surface potential barrier and the repulsive potential barrier of the ion-induced potential). At present, however, we are not sure that our model can reproduce such subtle effects. Thus, further research will be done to ensure that this effect is not accidental.
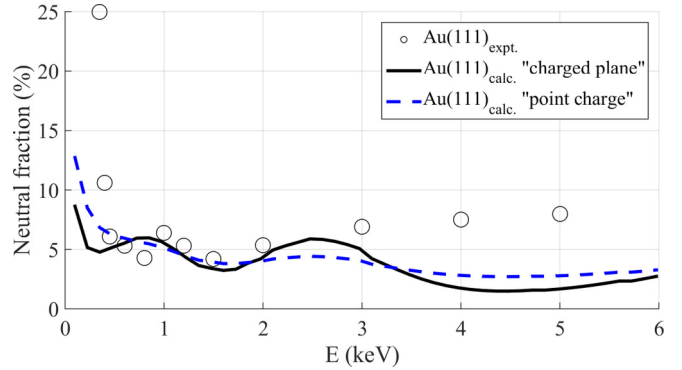
In addition, one should note the discrepancy between the results of calculation and the experimental data for $E > 3$ keV. The probable reason is that we do not take into account the ion energy level downward shift at small distances ($z_{ion} < 4$ a.u.), which is caused by short-range interactions [75]. First-principles quantum-mechanical calculations, which take into account short-range interactions [43,45], can give better results for energies greater than 3 keV.

IV. CONCLUSIONS

Finally, we have reported on the importance of an appropriate description of the ion-induced polarization charge in modeling of the resonant neutralization of positive ions on metal surfaces. Traditionally, it was taken into account as a point negative charge, located symmetrically to the image plane. Such an approach describes the ion level shift near the metal surfaces and gives reasonable values of the alkali-metal ion neutralization probability on the surfaces with a projected band gap. We have shown that the ion-induced charge is better described by means of a negatively charged plane located near the surface. This charged plane forms a potential barrier, the inclusion of which in the numerical model significantly reduces the calculated electron transfer probability and allows us to reach a quantitative agreement with experimental data for free-electron surfaces.

We have proposed an empirical ion-induced potential $\Delta V_{e-surf}(\boldsymbol{r})$, which includes the repulsive potential barrier in the image plane. The single fitting parameter of the proposed ion-induced potential was approximated only for one point of the energy dependence of the Na^+ neutralization probability on Cu(110), while the calculated energy dependence of the Na^+ neutralization probability is in quantitative agreement with experimental results for the energy range 0–3 keV for both Cu(110) and Au(111) surfaces. This is a strong argument to account for the repulsive potential barrier, arising due to the ion-induced polarization surface charge. Note that the relative error was about 50% in previous calculations of Na^+ neutralization on Cu(110).

The ion-induced potential and the electron self-attraction potential generate a potential well, where ion-induced states can arise. These states have a different nature from that of image potential states and extrinsic surface states caused by adsorbates. "Ordinary" image potential states arise only on surfaces with a projected band gap, while ion-induced states should also exist for the free-electron surfaces. The adsorbate-induced surface states are related to the strong interference between the atomic orbitals of the adsorbate and the bulk atoms, while ion-induced states arise due to the charge induced by the positive ion. We expect that, like image potential states, ion-induced states can be observed by means of inverse photoemission [59,83]. Note that ion-induced states should be more "detectible" in the case of multicharged ions [80].

Also, we have shown that inclusion of the repulsive potential barrier strongly affects resonant charge transfer in the case of free-electron metal surfaces and positive projectiles. For example, the traditional picture of projectile state decay is that the active electron moves along the normal deep into the metal and occupies 3D bulk states; the occupation of the projectile state decays exponentially. If one properly accounts for the charge induced by the positive ion, the electron exhibits partial reflection from the repulsive potential barrier generated by the ion-induced charge. As a result, the projectile's state decay occurs via ion-induced states, and the occupation of the projectile state exhibits oscillations. Such a picture is similar to RCT with metal surfaces with a projected band gap, where the electron exchange occurs via surface states.

ACKNOWLEDGMENTS

[1] Yu. V. Martynenko, Radiat. Eff. Defects Solids **20**, 211 (1973).

[2] I. F. Urazgil'din, Phys. Rev. B **47**, 4139 (1993).

[3] A. Tolstogouzov, S. Daolio, and C. Pagura, Surf. Sci. **441**, 213 (1999).

[4] A. Tolstogouzov, S. Daolio, and C. Pagura, Nucl. Instrum. Methods B **183**, 116 (2001).

[5] S. S. Elovikov, E. Yu. Zykova, A. S. Mosunov, A. A. Semyonov, I. I. Shkarban, and V. E. Yurasova, Bull. Russ. Acad. Sci.: Phys. **66**, 558 (2002).

[6] L. D. Bogomolova, A. M. Borisov, V. A. Kurnaev, and E. S. Mashkova, Nucl. Instrum. Methods B **212**, 164 (2003).

[7] A. S. Mosunov, Y. A. Ryzhov, I. I. Shkarban, V. E. Yurasova, and E. Yu. Zykova, Radiat. Eff. Defects Solids **162**, 401 (2007).

[8] A. V. Solov'yov, E. Surdutovich, E. Scifoni, I. Mishustin, and W. Greiner, Phys. Rev. E **79**, 011909 (2009).

[9] L. S. Alarcón, L. Chen, V. A. Esaulov, J. E. Gayone, E. A. Sánchez, and O. Grizzi, J. Phys. Chem. C **114**, 19993 (2010).

[10] L. Chen, J. Shen, J. E. Valdés, P. Vargas, and V. A. Esaulov, Phys. Rev. A **83**, 032901 (2011).

[11] H. Zhou, L. Chen *et al.*, Phys. Rev. A **85**, 014901 (2012).

[12] K. A. Tolpin, V. I. Bachurin, and V. E. Yurasova, Nucl. Instrum. Methods B **273**, 76 (2012).

[13] L. Chen, B. Ding, Y. Li, S. Qiu, F. Xiong, H. Zhou, Y. Guo, and X. Chen, Phys. Rev. A **88**, 044901 (2013).

[14] M. W. Ullah, A. Kuronen, F. Djurabekova, K. Nordlund, A. I. Titov, and P. A. Karaseov, Vacuum **105**, 88 (2014).

[15] A. A. Shemukhin, A. V. Nazarov, Yu. V. Balakshin, and V. S. Chernysh, Nucl. Instrum. Methods B **354**, 274 (2015).

[16] N. N. Andrianova, A. M. Borisov, E. S. Mashkova, and V. I. Shulga, J. Surface Invest. X-ray, Synch. Neutron Techn. **10**, 412 (2016).

[17] N. V. Mamedov, D. N. Sinelnikov, V. A. Kurnaev, D. V. Kolodko, and I. A. Sorokin, Vacuum **148**, 248 (2018).

[18] R. Brako and D. M. Newns, Rep. Prog. Phys. **52**, 655 (1989).

[19] H. Shao, D. C. Langreth, and P. Nordlander, in *Low Energy Ion-Surface Interactions*, edited by J. W. Rabalais (Wiley, New York, 1994).

[20] H. H. Brongersma, M. Draxler, M. de Ridder, and P. Bauer, Surf. Sci. **62**, 63 (2007).

[21] X. He, W. Zhou, Z. Y. Wang, Y. N. Zhang, J. Shi, R. Q. Wu, and J. A. Yarmoff, Phys. Rev. Lett. **110**, 156101 (2013).

[22] C. V. Cushman, P. Bruner, J. Zakel, G. H. Major, B. M. Lunt, N. J. Smith, T. Grehl, and M. R. Linford, Anal. Meth. **8**, 3419 (2016).

[23] I. K. Gainullin, Surf. Sci. **677**, 324 (2018).

[24] H. Winter, Phys. Rep. **367**, 387 (2002).

[25] A. G. Borisov, D. Teillet-Billy, and J. P. Gauyacq, Phys. Rev. Lett. **68**, 2842 (1992).

[26] U. Thumm, A. Bárány, H. Cederquist, L. Hägg, and C. J. Setterlind, Phys. Rev. A **56**, 4799 (1997).

[27] J. J. Ducrée, F. Casali, and U. Thumm, Phys. Rev. A **57**, 338 (1998).

[28] P. Kürpick and U. Thumm, Phys. Rev. A **58**, 2174 (1998).

[29] E. Y. Usman, I. F. Urazgil'din, A. G. Borisov, and J. P. Gauyacq, Phys. Rev. B **64**, 205405 (2001).

[30] I. K. Gainullin, E. Yu. Usman, Y. W. Song, and I. F. Urazgil'din, Vacuum **72**, 263 (2003).

[31] H. Chakraborty, T. Niederhausen, and U. Thumm, Phys. Rev. A **69**, 052901 (2004).

[32] H. Chakraborty, T. Niederhausen, and U. Thumm, Phys. Rev. A **70**, 052903 (2004).

[33] G. F. Liu, Z. Sroubek, and J. A. Yarmoff, Phys. Rev. Lett. **92**, 216801 (2004).

[34] I. K. Gainullin, E. Yu. Usman, and I. F. Urazgildin, Nucl. Instrum. Methods B **232**, 22 (2005).

[35] A. R. Canario, T. Kravchuk, and V. A. Esaulov, New J. Phys. **8**, 227 (2006).

[36] B. Bahrim, B. Makarenko, and J. W. Rabalais, Surf. Sci. **594**, 62 (2005).

[37] I. K. Gainullin and I. F. Urazgildin, Phys. Rev. B **74**, 205403 (2006).

[38] B. Obreshkov and U. Thumm, Phys. Rev. A **74**, 012901 (2006).

[39] D. K. Shestakov, T. Yu. Polivnikova, I. K. Gainullin, and I. F. Urazgildin, Nucl. Instrum. Methods B **267**, 2596 (2009).

[40] A. Schmitz, J. Shaw, H. S. Chakraborty, and U. Thumm, Phys. Rev. A **81**, 042901 (2010).

[41] L. Chen, J. Shen, J. Jia, T. Kandasamy, K. Bobrov, L. Guillemot, J. D. Fuhr, M. L. Martiarena, and V. A. Esaulov, Phys. Rev. A **84**, 052901 (2011).

[42] E. R. Amanbaev, I. K. Gainullin, E. Yu. Zykova, and I. F. Urazgildin, Thin Solid Films **519**, 4737 (2011).

[43] C. Meyer, F. Bonetto, R. Vidal, E. A. García, C. Gonzales, J. Ferrón, and E. C. Goldberg, Phys. Rev. A **86**, 032901 (2012).

[44] B. Obreshkov and U. Thumm, Phys. Rev. A **87**, 022903 (2013).

[45] L. Gao, Y. Zhu, Y. Shi, P. Liu, Y. Xiao, G. Li, Y. Liu, V. A. Esaulov, X. Chen, L. Chen, and Y. Guo, Phys. Rev. A **96**, 052705 (2017).

[46] J. Shaw, D. Monismith, Y. Zhang, D. Doerr, and H. S. Chakraborty, Phys. Rev. A **98**, 052705 (2018).

[47] C. Salvo, P. Karmakar, and J. Yarmoff, Phys. Rev. B **98**, 035437 (2018).

[48] Y. Xiao, Y. Shi, P. Liu, Y. Zhu, L. Gao, Y. Guo, L. Chen, X. Chen, and V. Esaulov, Nucl. Instrum. Methods B **450**, 73 (2019).

[49] J. Los and J. J. C. Geerlings, Phys. Rep. **190**, 133 (1990).

[50] J. Burgdorfer, in *Review of Fundamental Processes and Applications of Atoms and Ions*, edited by C. D. Lin (World Scientific, Singapore, 1993).

[51] U. Thumm, in *Ion-surface Interactions*, edited by J. Burgdorfer, J. S. Cohen, S. Datz, and C. R. Vane, Book of Invited Papers, XXII, ICPEAC, Santa Fe, NM (Rinton, Princeton, NJ, 2002).

[52] V. A. Esaulov, in *Low Energy Ion Scattering and Recoiling Spectroscopy in Surface Science*, edited by G. Bracco and B. Holst, Surface Science Techniques, Springer Series in Surface Sciences Vol. 51 (Springer, Berlin, 2013).

[53] T. Hecht, H. Winter, A. G. Borisov, J. P. Gauyacq, and A. K. Kazansky, Phys. Rev. Lett. **84**, 2517 (2000).

[54] T. Hecht, H. Winter, A. G. Borisov, J. P. Gauyacq, and A. K. Kazansky, Faraday Discuss. **117**, 27 (2000).

[55] S. G. Davison and M. Steslicka, *Basic Theory of Surface States* (Clarendon Press, Oxford, 1992).

[56] K. Oura, V. G. Lifshifts, A. A. Saranin, A. V. Zotov, and M. Katayama, *Surface Science* (Springer-Verlag, Berlin, 2003).

[57] W. Shockley, Phys. Rev. **56**, 317 (1939).

[58] I. E. Tamm, Phys. Z. Sowiet Union **1**, 733 (1932).

[59] E. V. Chulkov, V. M. Silkin, and P. M. Echenique, Surf. Sci. **437**, 330 (1999).

[60] W. Berthold, U. Höfer, P. Feulner, E. V. Chulkov, V. M. Silkin, and P. M. Echenique, Phys. Rev. Lett. **88**, 056805 (2002).

[61] J. P. Gauyacq and A. G. Borissov, in *Quantum Dynamics of Complex Molecular Systems*, edited by D. A. Micha and I. Burghardt, Springer Series in Chemistry and Physics Vol. 83 (Springer, Berlin, Heidelberg, 2007), pp. 87–109.

[62] V. A. Ermoshin and A. K. Kazansky, Phys. Lett. A **218**, 99 (1996).

[63] A. R. Canário, A. G. Borisov, J. P. Gauyacq, and V. A. Esaulov, Phys. Rev. B **71**, 121401(R) (2005).

[64] I. K. Gainullin, Phys. Rev. A **95**, 052705 (2017).

[65] L. Guillemot and V. A. Esaulov, Phys. Rev. Lett. **82**, 4552 (1999).

[66] B. Bahrim, B. Makarenko, and J. W. Rabalais, Surf. Sci. **603**, 703 (2009).

[67] S. S. Tsirkin, S. V. Eremeev, and E. V. Chulkov, Surf. Sci. **604**, 804 (2010).

[68] I. K. Gainullin and M. A. Sonkin, Comput. Phys. Commun. **188**, 68 (2015).

[69] I. K. Gainullin, Comput. Phys. Commun. **210**, 72 (2017).

[70] I. K. Gainullin, Surf. Sci. **681**, 158 (2019).

[71] J. N. Bardsley, in *Case Studies in Atomic Physics*, edited by E. W. McDaniel and M. R. C. McDowell (Elsevier, North-Holland, 1974), Vol. 5, pp. 299–368.

[72] J. S. Cohen and G. Fiorentini, Phys. Rev. A **33**, 1590 (1986).

[73] P. J. Jennings, R. O. Jones, and M. Weinert, Phys. Rev. B **37**, 6113 (1988).

[74] I. K. Gainullin and M. A. Sonkin, Phys. Rev. A **92**, 022710 (2015).

[75] E. A. García, M. A. Romero, C. González, and E. C. Goldberg, Surf. Sci. **603**, 597 (2009).

[76] P. Nordlander and J. C. Tully, Phys. Rev. B **42**, 5564 (1990).

[77] L. D. Landau and E. M. Lifshitz, *Electrodynamics of Continuous Media* (Pergamon Press, Oxford, 1960).

[78] N. D. Lang and W. Kohn, Phys. Rev. B **7**, 3541 (1973).

[79] R. Ray and G. D. Mahan, Phys. Lett. A **42**, 301 (1972).

[80] A. Arnau, F. Aumayr, P. M. Echenique, M. Grether, W. Heiland, and J. Limburg *et al.*, Surf. Sci. Rep. **27**, 113 (1997).

[81] A. G. Borisov, A. K. Kazansky, and J. P. Gauyacq, Phys. Rev. Lett. **80** (1998) 1996.

[82] F. Wyputta, R. Zimny, and H. Winter, Nucl. Instrum. Methods B **58**, 379 (1991).

[83] F. J. Himpsel, Comments Cond. Mat. Phys. **12**, 199 (1986).